
MEASUREMENT AND INTERPRETATION OF THE SMALL STRAIN STIFFNESS OF BOŠTANJ SILTY SAND

GREGOR VILHAR and VOJKAN JOVIČIĆ

About the authors

Vojkan Jovičić
Institute of Mining, Geotechnology and Environment (IRGO)
Slovenčeva 93, 1000 Ljubljana, Slovenia
E-mail: vojkan.jovicic@irgo.si

corresponding author

Gregor Vilhar
Slovenian National Building and Civil Engineering Institute
(ZAG Ljubljana)
Dimičeva 12, 1000 Ljubljana, Slovenia
E-mail: gregor.vilhar@zag.si

Abstract

This paper presents measurements, and an interpretation of these measurements, based on the use of bender-element probes for Boštanj silty sand. The samples were prepared at different initial void ratios and isotropically compressed up to 5 MPa. The bender-element technique was used to determine the dynamic shear modulus (G_0) of the soils at very small strains. The multiple bender-element probes were shot at different excitation frequencies in order to increase the reliability of the measurements. The G_0 stiffness was determined by using three different techniques: a) the first-time arrival, b) the phase-change method and c) the cross-correlation method. The systematic differences observed between the G_0 values, calculated using the three techniques, are discussed. The variation of G_0 in the $\log G_0 - \log p'$ plane was evaluated for the Boštanj silty sand and compared with other sands.

keywords

silty sand, triaxial testing, small strain stiffness, bender elements, time-domain and frequency-domain measurements

1 INTRODUCTION

By using bender elements, the shear stiffness (G_0) of a material at very small strains ($\varepsilon < 10^{-5}$) can be measured during conventional laboratory tests. In the past few decades it was recognised that the so-called elastic stress-strain response of soils and soft rocks is highly non-linear and often anisotropic. The bender-element technique represents one of the ways of measuring the stiffness at the very beginning of this non-linearity and it can capture the anisotropic features of small strain stiffness.

The use of bender elements in geotechnics began in the late 1970s with Shirley and Hampton [22] and later with Dyvik and Madshus [10], who showed very good agreement between the results obtained by the bender elements and with resonant-column tests. The advantages of this method lie in its relatively simple installation, low cost and the non-destructive nature of the measurement. It was made possible to install bender elements as a complementary measurement technique in various types of laboratory equipment, such as triaxial cells, oedometers, direct shear, hollow cylinder, true triaxial, cubical cell and the resonant column apparatus, Fonseca et al. [12]. However, some problems concerning the proper use of the technique and the interpretation for the different installations have evolved; see, for example, [7, 23, 17].

The set-up for the bender-element test in a triaxial cell is presented in Figure 1. A bender element is a piezoceramic element made of two transversely poled plates that are bonded together. When one end of the element (the transmitter element in the figure) is fixed the excitation of the external voltage will make the opposite end move and the element will bend in the direction normal to the face of the plates. In ideal conditions the transmitter element, embedded in the soil sample, introduces a shear wave into it. Upon the arrival of the shear wave at the other end of the soil sample the receiver element will move and generate a small voltage, which is detected at the electrode and shown on an oscilloscope. The technique is based on a measurement of the arrival time

of the shear wave, assuming a plane-wave propagation, i.e., the time difference between the excitation of the transmitter and the excitation of the receiver element, as indicated in Figure 1.

On the basis of this assumption, the shear-wave velocity (v_s) can be calculated from the current travel distance of the wave (D) and the time of the arrival of the wave at the receiver element (t_{arr}), according to Equation

(A.1) in the Appendix. The distance D was taken as the current tip-to-tip distance of the bender elements, which is experimentally supported by Dyvik and Madshus [10], Brignoli et al. [6], Viggiani and Atkinson [23], and Fernandez [11]. The shear modulus at a very small strain (G_0) can be calculated from the current bulk density of the material (ρ) and the previously calculated shear-wave velocity, according to Equation (A.2).

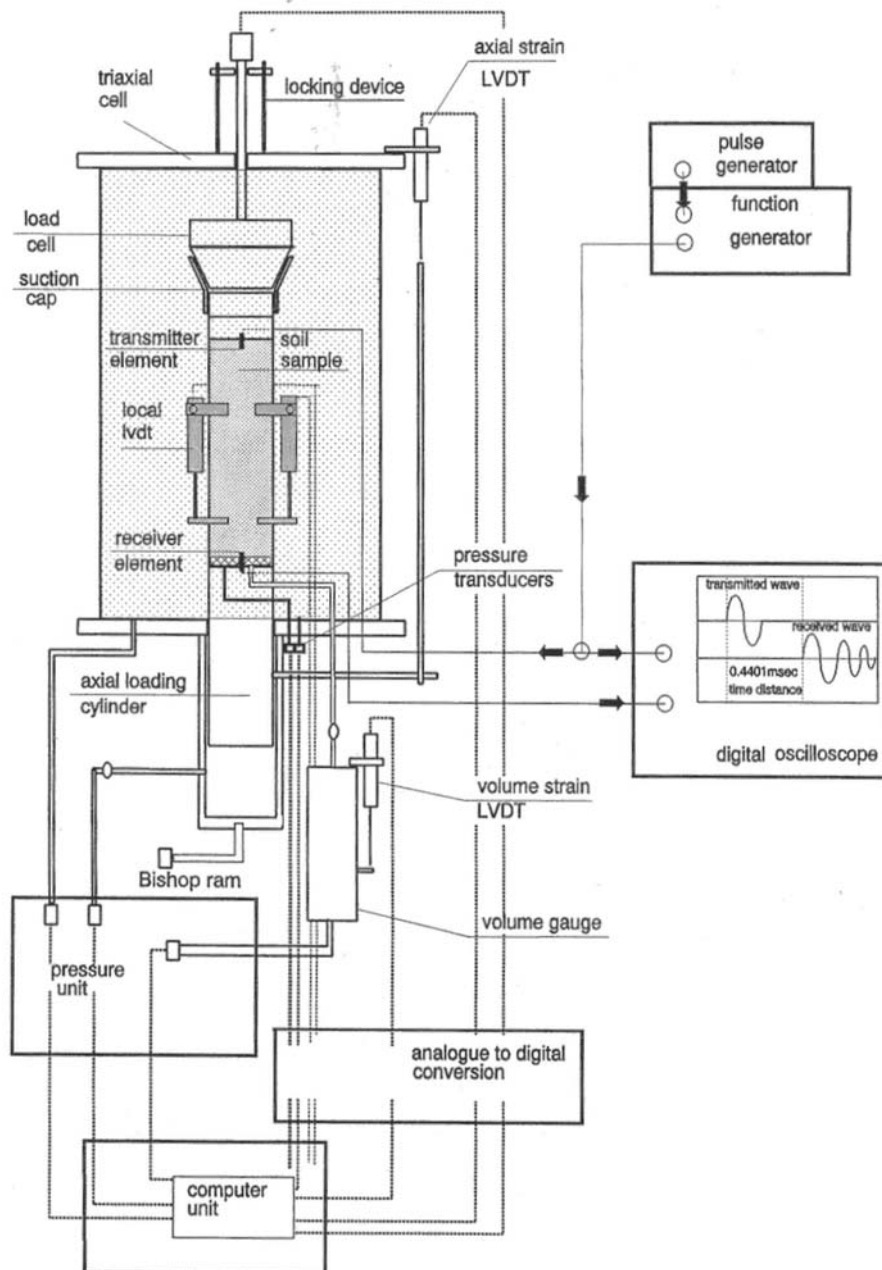


Figure 1. The set-up for the bender-element test in a triaxial cell (after Jovičić [16]).

2 MATERIAL AND LABORATORY TESTING PROCEDURE

The material used for this research was a silty sand from a railway-line embankment near the town of Boštanj, Slovenia. Some aspects of the static and dynamic behaviour of the same material can be found in Lenart [19]. The sieve and sedimentation analyses shown in Figure 2 revealed that Boštanj silty sand consists of fine sand with 30% of non-plastic silt. It is a well-graded material with a uniformity coefficient $C_u = 0.721$ and a mean particle size $D_{50} = 0.11$ mm. The particle specific gravity G_s is 2.75.

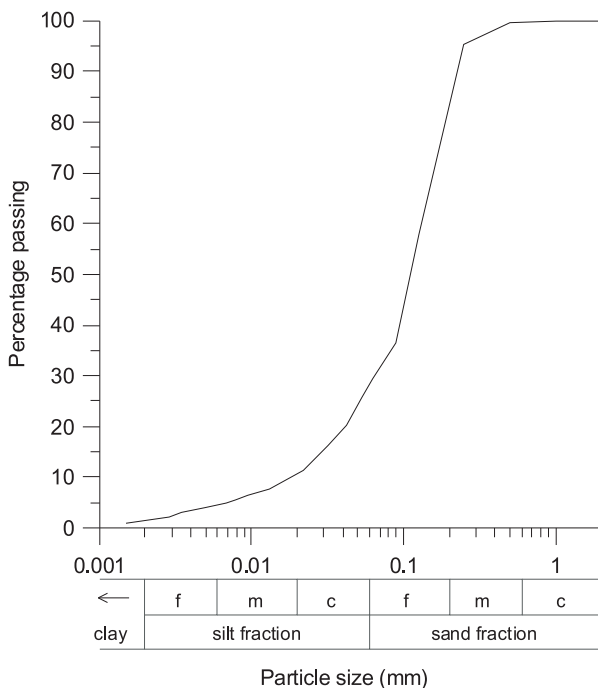


Figure 2. Particle size distribution of the Boštanj silty sand.

In total, nine triaxial tests were carried out with the aim being to measure the effect of the density and the stress state on G_0 in isotropic compression. The samples were prepared at different initial void ratios using the moist-tamping method.

A predetermined amount of slightly wet material, with a water content of $w = 10\%$, was placed in a mould in 10 equal weight portions. Each portion was compacted with a flat tamper of a circular shape with a diameter equal to half of the sample's diameter to achieve the desired equal height of each layer. The samples were saturated by raising the pore-water pressure to reach B values higher than 0.95. Two types of triaxial apparatus were used, i.e., a standard

pressure apparatus achieving a maximum cell pressure of 0.8 MPa and a high-pressure triaxial apparatus achieving a cell pressure of up to 5 MPa, both at Imperial College Soil Mechanics Laboratory. Four tests were performed on the standard pressure apparatus and five tests on the high-pressure apparatus. The schematic diagrams of both apparatus are similar to that shown in Figure 1.

The standard pressure cell is a Bishop & Wesley type of cell. It is a fully computer-controlled cell, equipped with local axial strain-measuring inclinometers, directly glued to the sides of the sample. The cell was also fitted with a pair of bender elements, mounted in the top-cap and bottom-pedestal for measuring the velocity of vertically propagating, horizontally polarised, shear waves. The dimensions of the bottom element were width (13.0 mm) x sample protrusion (4.5 mm) x thickness (1.5 mm), and of the top element were width (15.0 mm) x sample protrusion (4.5 mm) x thickness (1.5 mm). The sample dimensions were around 38.5 mm in diameter and 90.0 mm in height. Such a high slenderness ratio of was used because of the existing mould dimensions.

The high-pressure triaxial cell was capable of applying a maximum radial stress of 5 MPa. Both the cell and axial stresses have alternative low- and high-pressure systems. This cell is also fully computer controlled. A pair of axial LVDTs [9] and a LVDT-fitted radial belt were glued to the sides of the sample. A pair of bender elements for measuring the velocity of axially propagated shear waves was also installed in this cell, having the following dimensions: the bottom element, width (11.5 mm) x sample protrusion (3.8 mm) x thickness (1.5 mm), and the top element, width (11.5 mm) x sample protrusion (5.8 mm) x thickness (1.5 mm). The sample dimensions were around 50 mm in diameter and 110 mm in height.

3 INTERPRETATION OF THE BENDER-ELEMENT TEST ON THE SAMPLES OF BOŠTANJ SILTY SAND

3.1 INTERPRETATION TECHNIQUES

The main reason for the difficulties in the interpretation of the bender-element test was the lack of understanding of the interaction of the bender-element system and the soil sample during the measurement. Most often, this interaction results in dispersion, meaning that the initial excited wave at the transmitter element spreads into different components, propagating at different speeds,

frequencies and along different paths. The presence of the mixture of the components could therefore mask the detection of the actual arrival of the shear wave at the receiver element, which characterises the shear velocity of the medium. Furthermore, to what extent the output signal appears distorted depends directly on the number of vibration modes excited by the propagated wave.

The most widely dealt type of dispersion has been the near-field effect. It is usually recognised as an initial drop in signal, having a different polarity than the driving signal, as shown in Figure 3. Different criteria have

been proposed in order to minimize this effect, mostly in terms of the minimum number of shear wavelengths between the transducers, see, for example, [21, 17, 4]. Taking into account such criteria, the experimental and numerical analyses indicate that other types of dispersion are also supposed to have a strong influence on the observed distortion of the bender-element signals (Arroyo et al. [4]), in particular those still evident at higher frequencies than the near-field criteria would predict. Current knowledge suggests that there is also an evident geometrical effect on the propagation pattern in the bender-element system, see, for example, [20, 3].

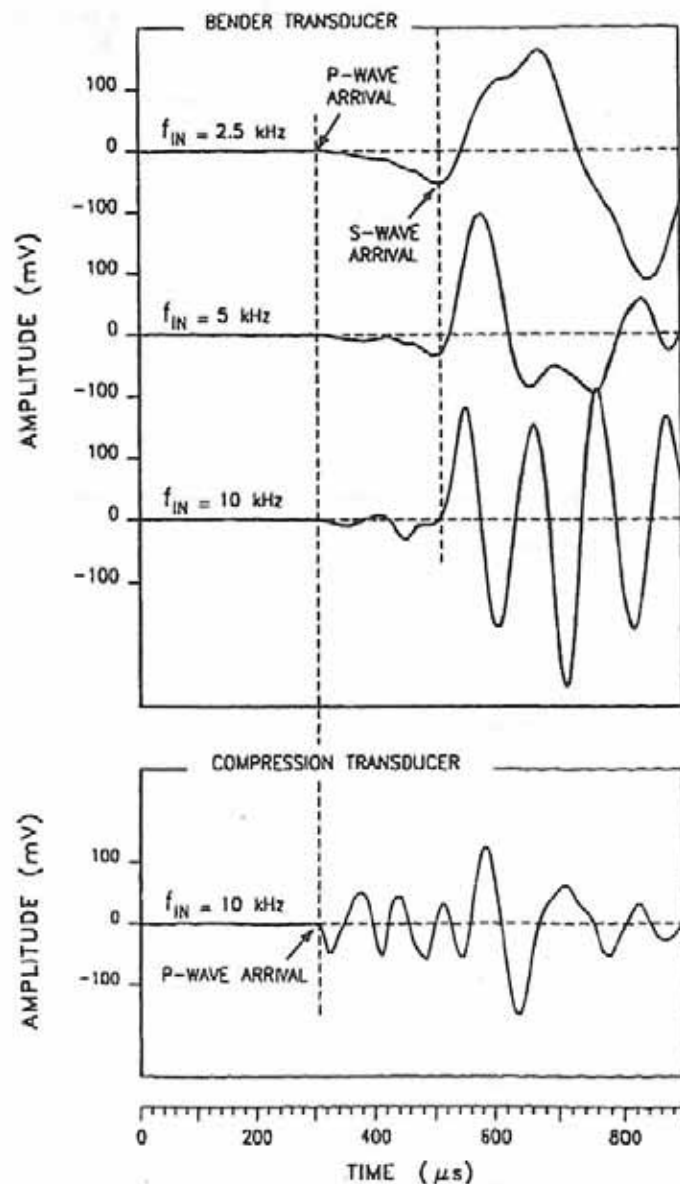


Figure 3. Near-field effect and the detection of the arrival of the compressive components before the actual shear wave with the compression transducer (after Brignoli et al. [6]).

In terms of interpretation, the methods can be classified into two main groups: the time-domain methods and the frequency-domain methods. In the time domain, the user visually determines the arrival time of the shear wave by examining the output and input signal voltages versus time. In the frequency domain, the stored input and output signals are transformed and manipulated in the frequency domain.

Both groups of interpretation methods were focused on minimizing the influence of the dispersion effects. In the time domain this can be achieved by adapting the frequency of the transmitted pulse. The most commonly used type of signal in the time domain is the single sine pulse, as it contains a predominant single frequency and this can help to avoid the near-field effect. The distortion of the right shape of the sine signal was shown experimentally to effectively reduce the near-field effect (Jovičić et al. [17]). The effectiveness of this type of pulse signals has also been proven numerically (Arroyo et al. [4]). All current time-domain methods rely on a visual identification of the arrival time of the shear wave, whereas different researchers have preferred different geometrical features of the output signal as an arrival point (e.g., the first rise of the signal, the first change of curvature, the first peak and the peak-to-peak between the input and output signals). However, the real physical meaning of the arrival time is the first rise of the received signal, and this is why the method was used here for the interpretation. The first change of the curvature or the peak-to-peak are the subject of an interpretation of how the receiver responded to the incoming wave, so that a variability between the results obtained from the different criterion/input signal combination is expected and can be substantial, as shown by Arroyo et al. [4] and Alvarado [1]. Concerning mostly the frequency-domain interpretation, the pulse signals along with the harmonic continuous signals at a constant frequency and linearly swept sine signals of different frequency ranges have also been used [13, 1, 12]. In the present study, the methods of first arrival and cross-correlation were employed in the time domain, while in the frequency domain, the phase-change method was used. All the methods are described in some detail, while the relevant equations are presented in the Appendix. In all the cases, the single sine pulses were used at different excitation frequencies from 1 to 50 kHz. The data were analysed using computer codes written in Matlab 7.3.

The main deficiency of all the interpretation methods is the subjectivity of the user involved in the interpretation of the shear-wave arrival time. There have been some attempts to make the interpretation more objective in the frequency domain using computer software (e.g.,

Fonseca et al. [12]), but the user still has to determine the proper frequency interval and decide among the calculated values of the time arrival. The level of reliability can be different, depending on the different test conditions or materials (Alvarado & Coop [2]). Therefore, the use of a combination of measurement and interpretation methods is proposed, leading to a higher level of confidence in the computed arrival time, whereas no single combination of interpretation criterion/selected input signal is universally accepted. The use of multiple methods has also been supported by the recent reports of Technical Committee TC29 of the ISSMGE [14,24].

Three different ways of interpreting the results were used along with the calculated error in G_0 : the first arrival time, the cross-correlation and the frequency-domain method of the phase change. The single-shot sine pulses have been used as the driving signals for both the time- and frequency-domain interpretations. Figure 4 shows the comparison of the transfer functions calculated using sine-pulse signals at different excitation frequencies and continuous sine signals of discretely varying frequencies for each point for Toyoura sand [1]. The transfer-function gain and the stacked phase are defined in the Appendix using Equations (A.6) and (A.7). In a certain frequency domain, i.e., between 6 and 12 kHz, a good match between the slope of the stacked phase against the frequency is found and, as will be explained later, the group time arrival can be easily calculated.

3.2 INTERPRETATION OF THE TIME-DOMAIN MEASUREMENT

In the time domain, the method of first arrival was used. The signals from the probes with different excitation frequencies in a certain stress state were collected on the same plot. The data were normalised and offset with respect to the beginning of the sent signals, as shown in Figure 5. Afterwards, the arrival time was estimated according to the well-pronounced sharp change in polarity in the same direction and of a similar shape to the input signal. It can be observed in Figure 5 that by increasing the input frequency to 20 kHz the change in the polarity becomes sharper. Higher frequencies are not relevant because of the poor coupling between the bender elements and the soil (the phenomena of overshooting, Jovičić et al. [17]), but are added to the plot as a reference.

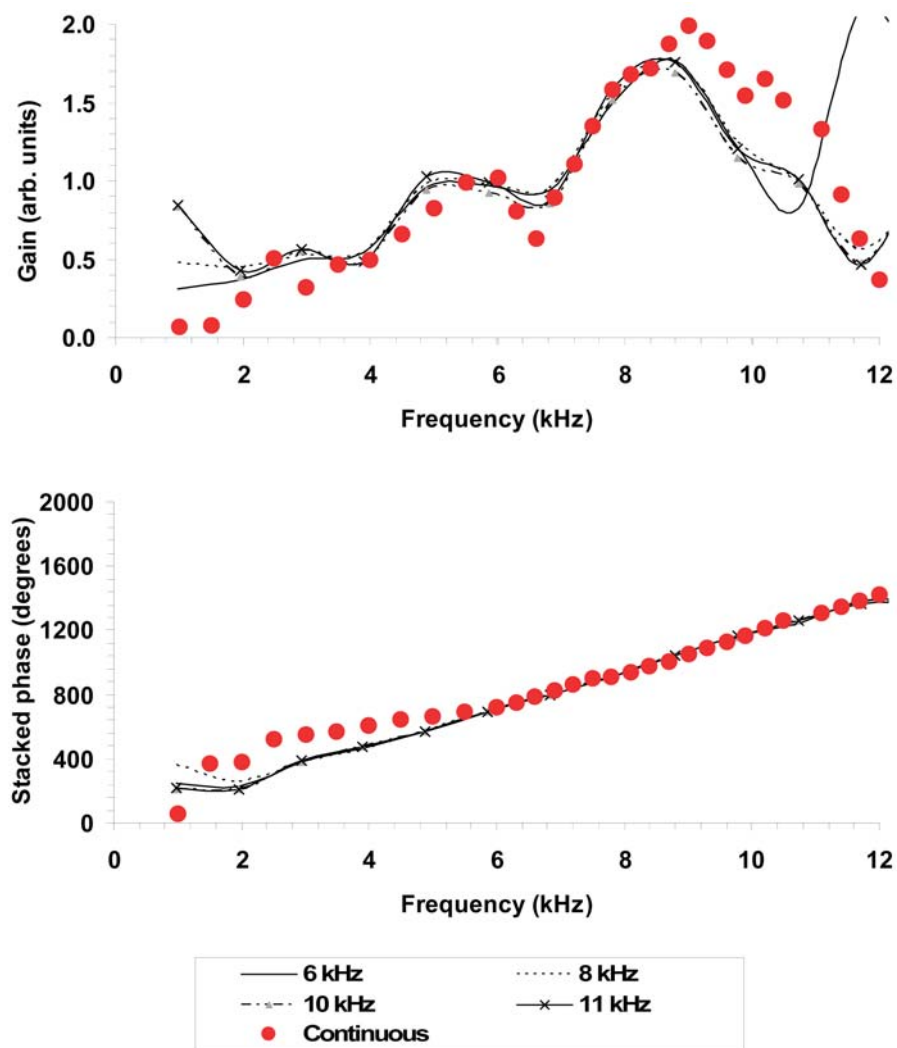


Figure 4. The good match of the transfer function for Toyoura sand at $p' = 220$ kPa, calculated from the sine pulse signals at different excitation frequencies and continuous sine signals with discretely varying frequencies (after Alvarado [1]).

By increasing the mean effective stress p' , the signals become more distorted, but, on the other hand, the arrival points, for certain frequencies, can be distinguished more easily (Figure 6). This method relies on two factors: a) the measurement should be taken at excitation frequencies that ensure a minimisation of the influence of the near-field effect and b) at this range of frequencies a comparison should be made for several different signals on the same plot. In this way the frequency-dependent patterns of the behaviour of the system can be visually recognised and the signal with the sharpest arrival pattern can be chosen to be relevant for the identification of the arrival point.

It can be seen in Figure 6 that the output signals have an initial bump of the same shape and polarity positioned almost at the same time as the bump of the input signals appears. The reason for these bumps is the leakage of the input signal through the conductive medium (i.e., the pore water) from the transmitter to the receiver, called the 'cross-talk' (Figure 7). The solution to this problem is usually the proper grounding of the elements. In our case, the contaminated parts of the signals were replaced by the uniformly distributed pseudo-random noise of small amplitude, using Matlab's rand function. This replacement only has an effect on the frequency-domain calculation, while the cross-talk part contaminates the frequency content of the output signal and, as such, affects the time-arrival calculation.

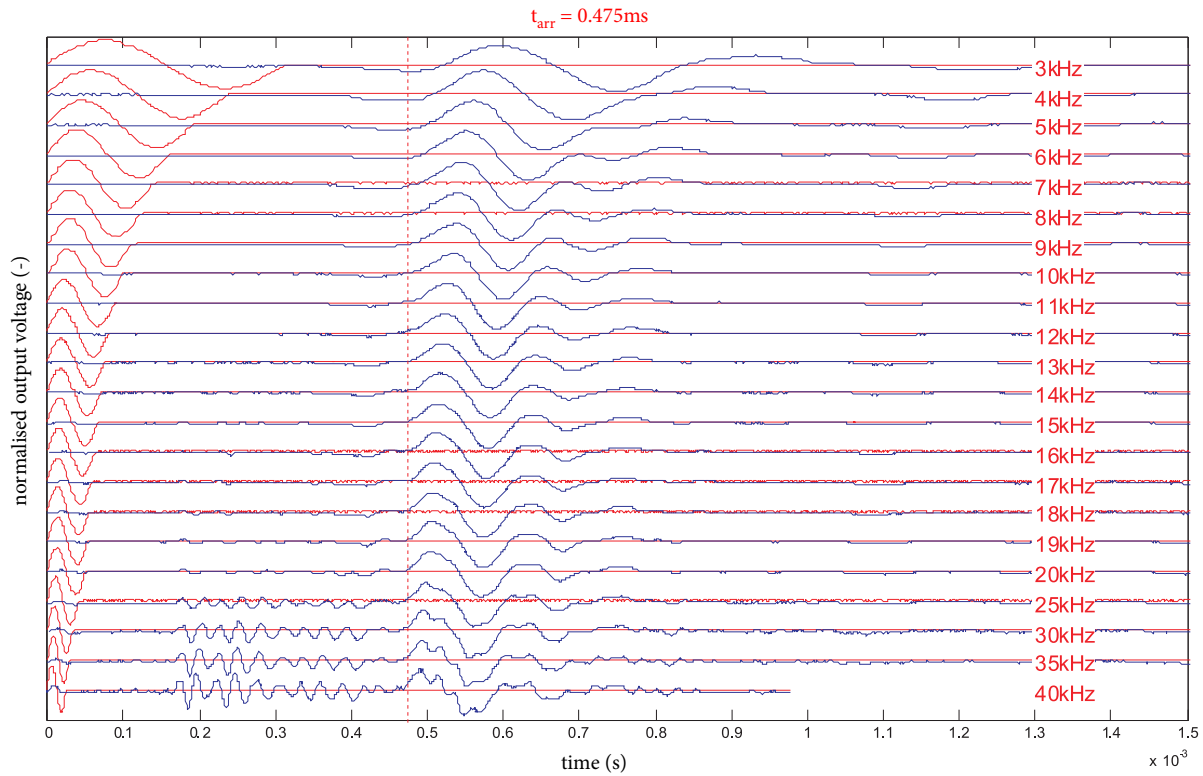


Figure 5. Input (red) and output (blue) signals from the bender-element probes for the sample BO-I-J at $p' = 200$ kPa. The increase in the sharpness of the arrival-time point with increasing frequency up to 20 kHz can be seen.

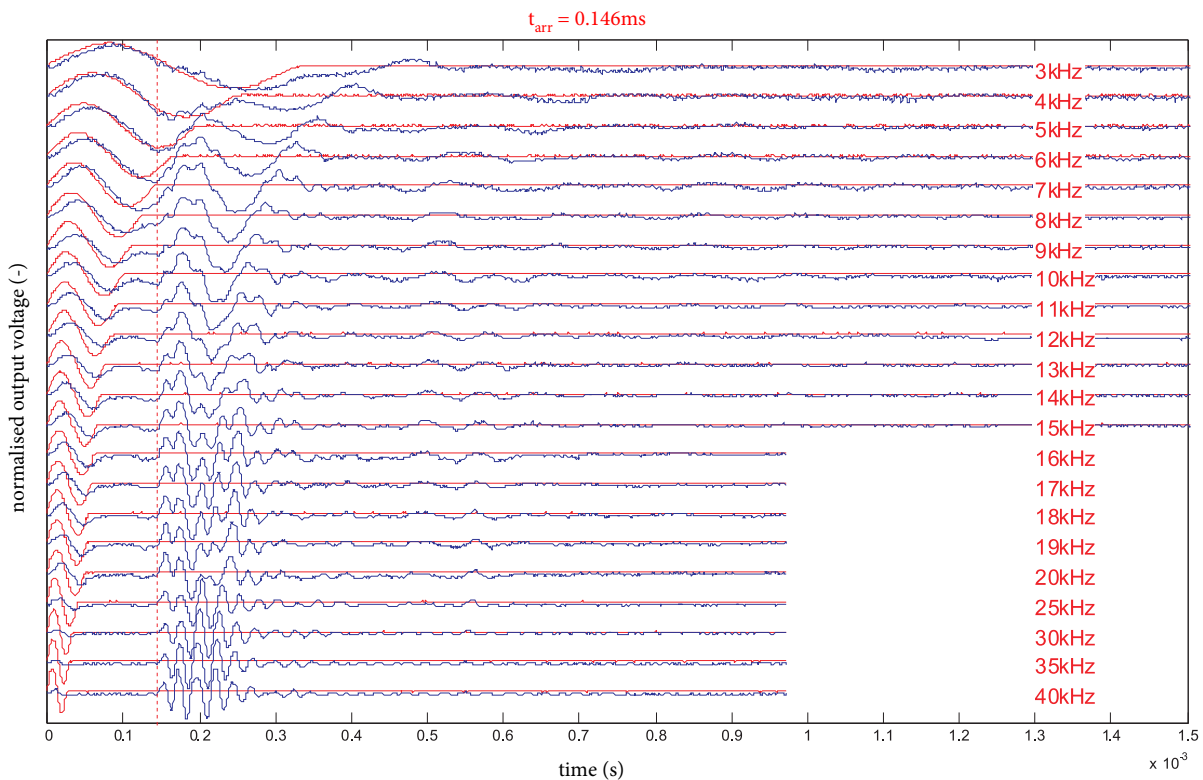


Figure 6. Input (red) and output (blue) signals from the bender-element probes for the sample BO-I-J at $p' = 4700$ kPa. Distorted signals due to high stresses and high density of the sample can be seen. The arrival time can be distinguished more easily.

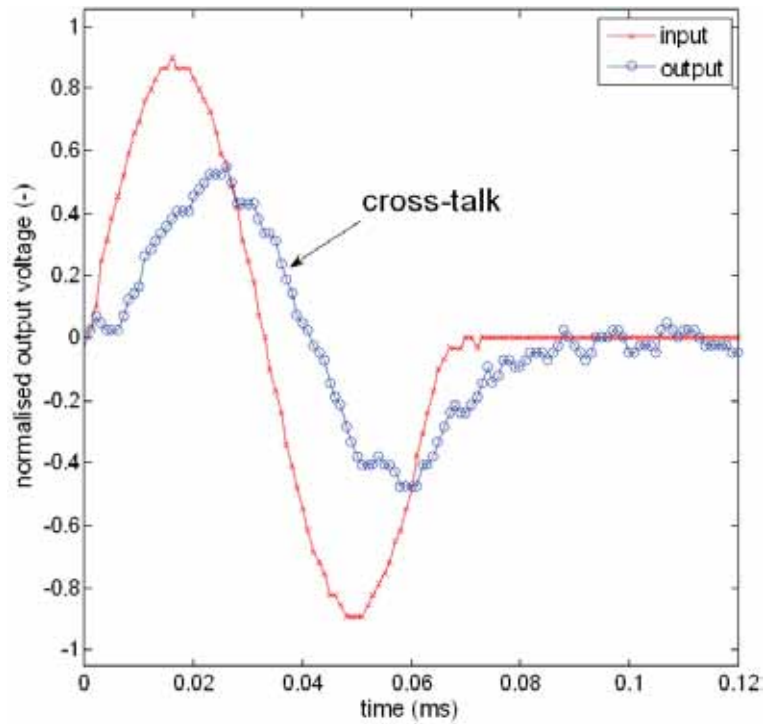


Figure 7. Contamination of the output signal with cross-talk.

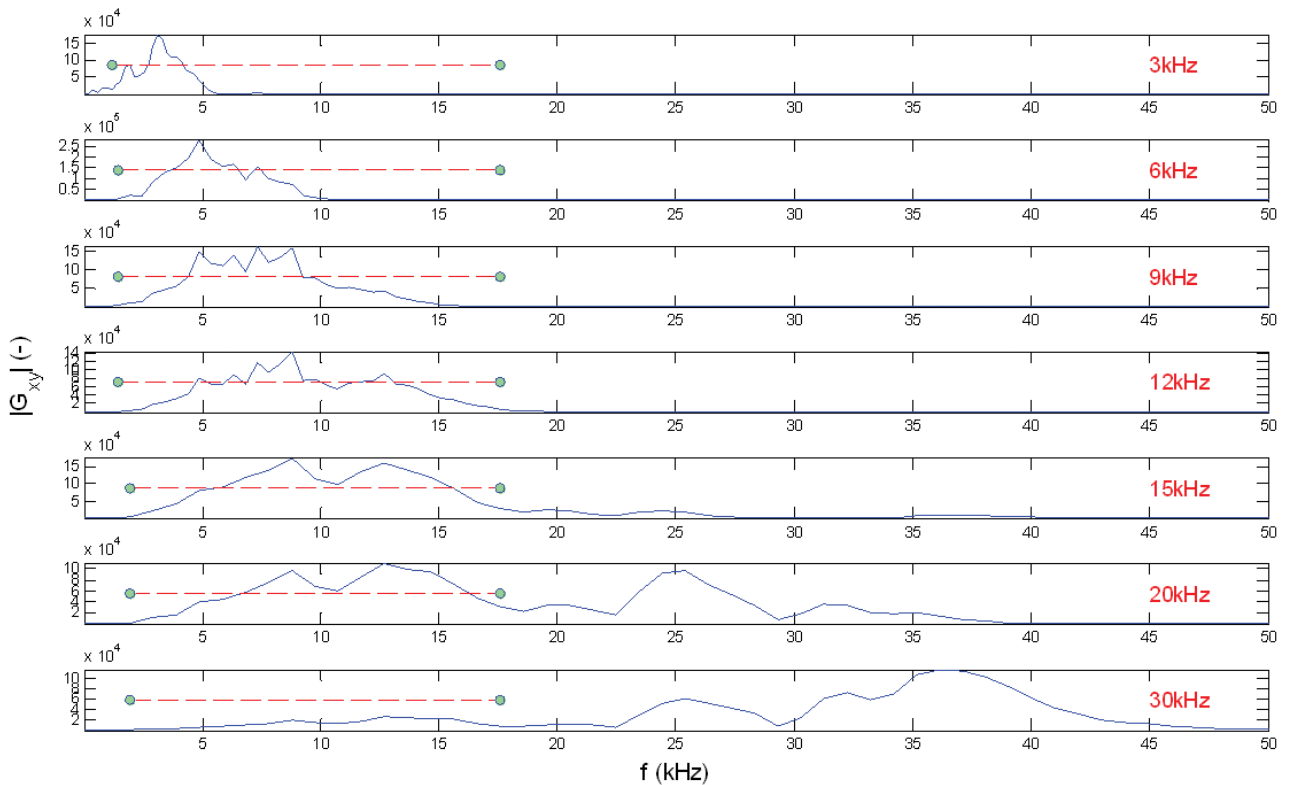


Figure 8. Cross spectrum magnitudes $|G_{xy}|$ versus frequency f for the sample BO-I-J at $p' = 1300$ kPa, using input sine-pulse signals at different frequencies (the values on the right-hand side of plots). The chosen frequency interval for the t_g calculation is also marked.

3.3 INTERPRETATION OF THE FREQUENCY-DOMAIN MEASUREMENTS

The frequency-domain method consists of interpreting the phase change between the transmitted and received signals. The whole input and output signals were transformed into the frequency domain using a fast Fourier algorithm (FFT). The analysis began by plotting the cross-power spectra magnitude $|G_{xy}|$ versus the frequency for selected signals at a chosen stress-state, as shown in Figure 8. The expression for G_{xy} can be found in Equation (A.4). At each frequency, the magnitude $|G_{xy}|$ is a product of the amplitudes of both signals at that frequency.

The analysis proceeded with the plots of the stacked (unwrapped) system phase factor ϕ versus frequency (Equation (A.7)) for all the chosen signals. Figure 9 shows only one such plot (at $f = 15\text{kHz}$) in order to clearly see the content. By plotting $|G_{xy}| - f$, the frequency ranges are observed common to both the input and output signals. The widest possible frequency interval covering the linear relation of $\phi - f$ is then chosen (marked by two blue dots connected with the dashed line in Figures 8 and 9). The chosen interval should cover most of the major amplitudes in the $|G_{xy}| - f$ plots, but the deficiency of the methods is that a slight change in the frequency interval could cause

a big change in the calculated arrival time. Therefore, to increase the robustness of the approach, the widest, still highly linear, interval of f in the $\phi - f$ plot, covering most of the major amplitudes in $|G_{xy}| - f$, must be chosen. From the value of the slopes $\frac{d\phi}{df}$ of the least-squares-fit lines of the chosen frequency interval, the group time arrivals (t_g) were calculated (Equation (A.10)).

The tangents were calculated in the linear range of the strong amplitudes of the transmitted and received signals, meaning that the calculated group time arrival t_g is supposed to be the arrival time of the main shear wave packet and, therefore, the group time arrival is assumed to be equal to the shear-wave time arrival ($t_g \cong t_{arr}$).

All of the signals were then plotted in the time domain along with the marked positions of the calculated group arrival times (Figure 10). The proper value of t_g was then chosen using Figure 8 and all of the $\phi - f$ plots with superimposed linear trends at chosen intervals. The correlation coefficient (ρ_{xy}) between the linear trend and the data can serve as a guide for choosing the right value. In the presented case the t_g values from the signals with 9, 12, 15 and 20 kHz were of the best quality. The signal with the frequency of 30 kHz is likely to experience overshooting because of the high frequency;

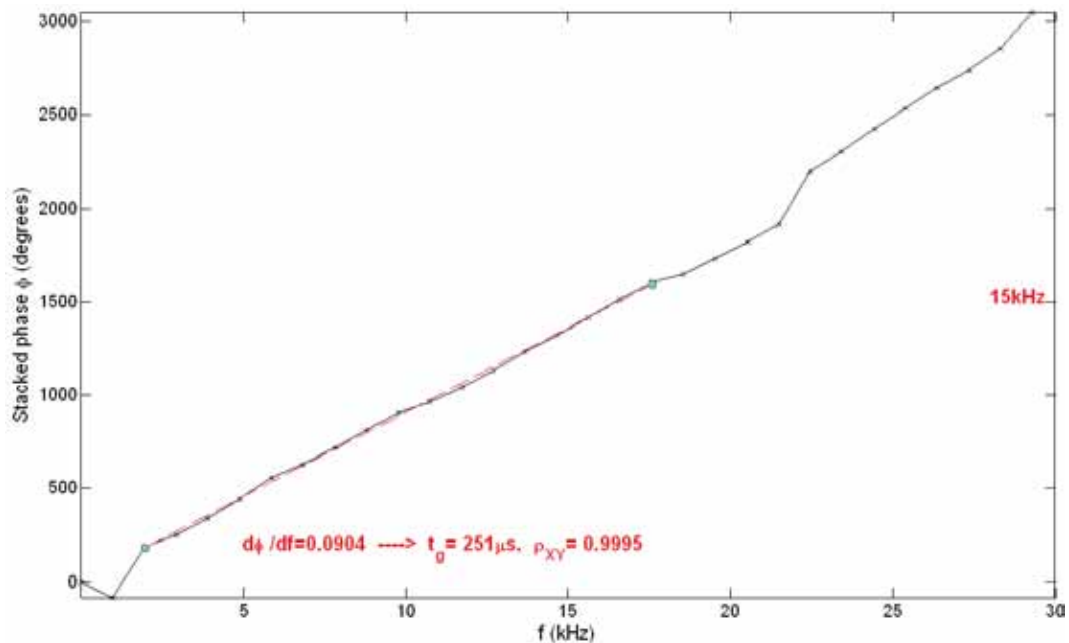


Figure 9. Stacked (unwrapped) system phase factor ϕ versus frequency f for the sample BO-I-J at $p' = 1300\text{ kPa}$, using the input sine pulse signal at 15 kHz . (The properly chosen frequency interval covering the widest linear range is also shown, along with the value of the slope $\frac{d\phi}{df}$, the group time arrival t_g and the correlation coefficient ρ_{xy} between the data and the shown linear trend.)

therefore, it is disregarded from the group. The average value of t_g for the four candidate signals could be taken, or the $t_g = 0.251$ (signal at 15kHz) was chosen due to the highest correlation coefficient. The $\phi - f$ plot of the 15-kHz signal is shown in Figure 9. A good match for the linear least-squares trend and the data can be observed.

It can be seen from Figure 10 that the calculated group arrival time t_g of the four appropriate signals along with the frequency intervals does not depend much on the excitation frequency. The very different values of t_g for the signals of 3 and 6 kHz are likely to be due to the very dispersive nature of both signals caused by the presence of the near-field effect in the receiving wave. Figure 11 demonstrates this, showing the $\phi - f$ plot for 6 kHz along with the poor linear trend. If the frequency interval is changed to cover the narrower range of 2–12 kHz, the calculated t_g value is 0.265 ms and the coefficient of correlation is substantially improved to 0.9959.

3.4 INTERPRETATION OF THE CROSS-CORRELATION MEASUREMENTS

The arrival times t_{arr} were also calculated using the cross-correlation function $CC_{XY}(t)$ (Equation (A.11)). Using this method, it is assumed that the shapes of the transmitted and received signals are very similar, i.e., of equal frequency content. The main deficiency of this method is that this is not necessarily the case in the bender-element measurement, as the shape of the received signal is, by definition, far more complex than the transmitted one. Nevertheless, due to its simplicity of use, it has been chosen as a complementary method in this research.

The cross-correlation function was plotted for the chosen signals of the phase-change method. Figure 12 shows the cross-correlation plots of the data from Figure 10, along with the position of the calculated group arrival times t_g from the phase-change method. It can be seen that for the signals at relevant frequencies (9, 12, 15 and 20 kHz) the peaks of the cross-correlation function are close to the positions of the group arrival times.

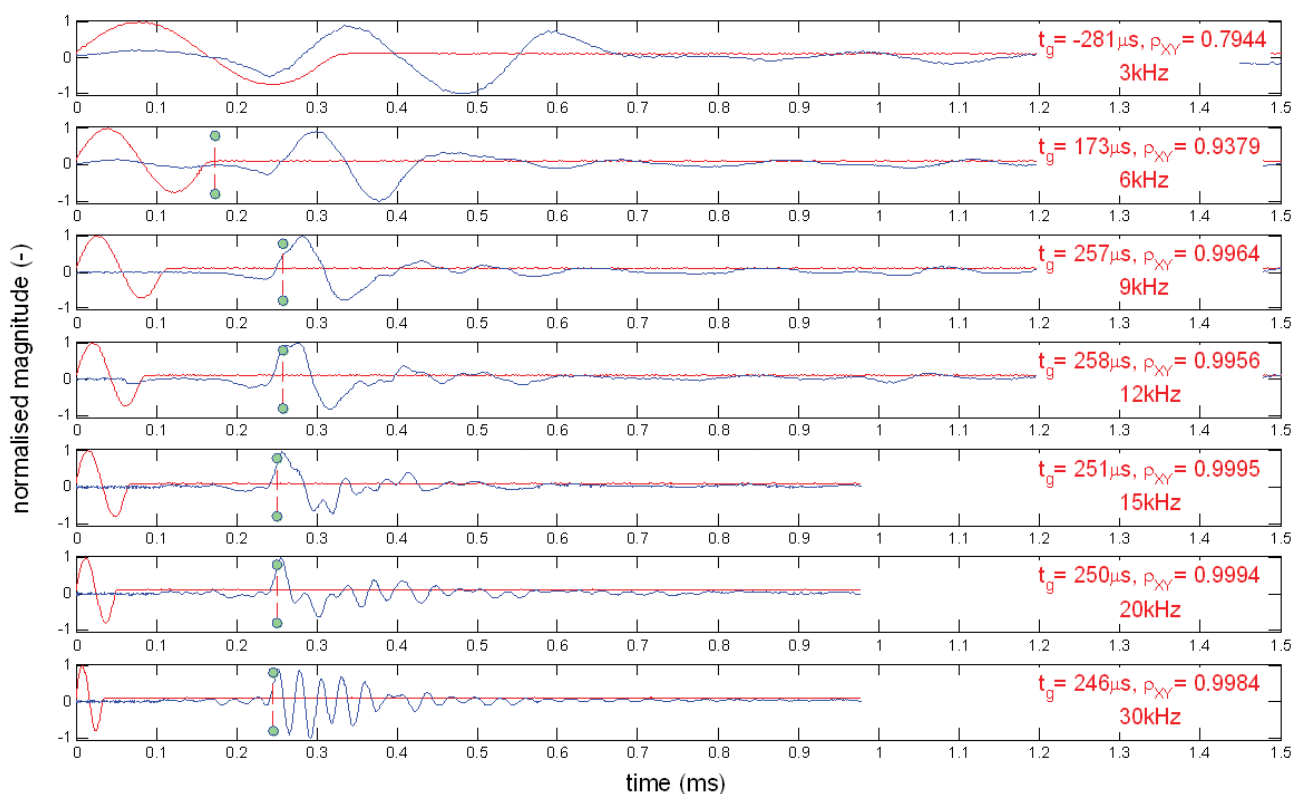


Figure 10. Input and output signals along with the positions of the calculated group arrival times t_g (sample BO-I-J at $p' = 1300$ kPa). (On the right-hand side of each plot the values of the calculated group arrival time (t_g), the correlation coefficient (ρ_{xy}) between the linear trend and the stacked phase and excitation frequency (f) of the pulse are given.)

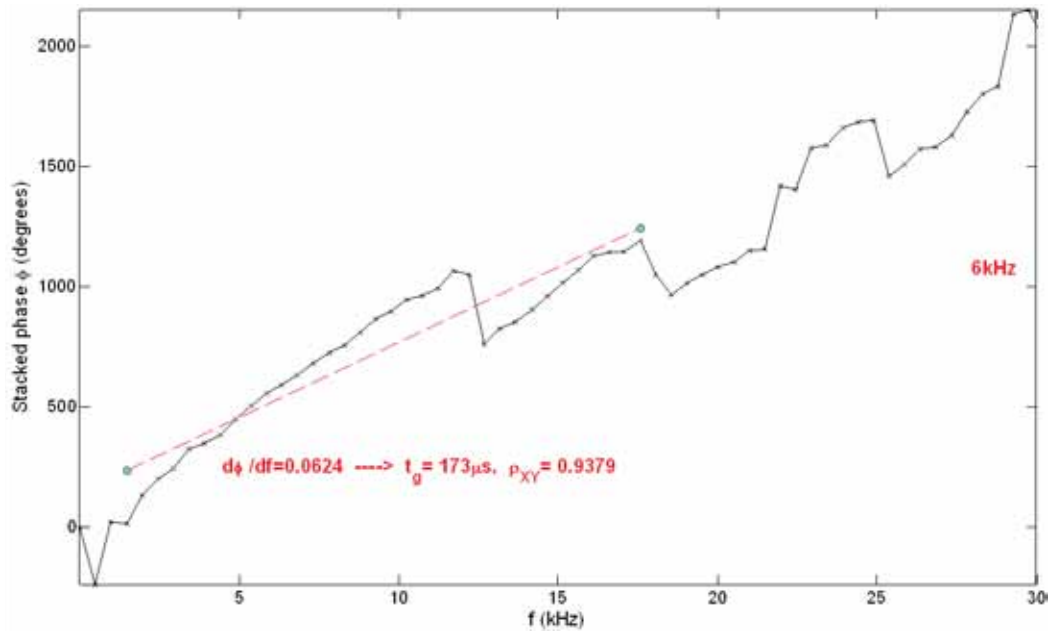


Figure 11. Stacked phase ϕ of the transfer function versus frequency f for the sample BO-I-J at $p' = 1300$ kPa, using an input sine pulse signal at 6 kHz. (The poorly chosen frequency interval covering the widest linear range is also shown, along with the value of the slope $\frac{d\phi}{df}$, the group time arrival t_g and the correlation coefficient ρ_{xy} between the data and the shown linear trend.)

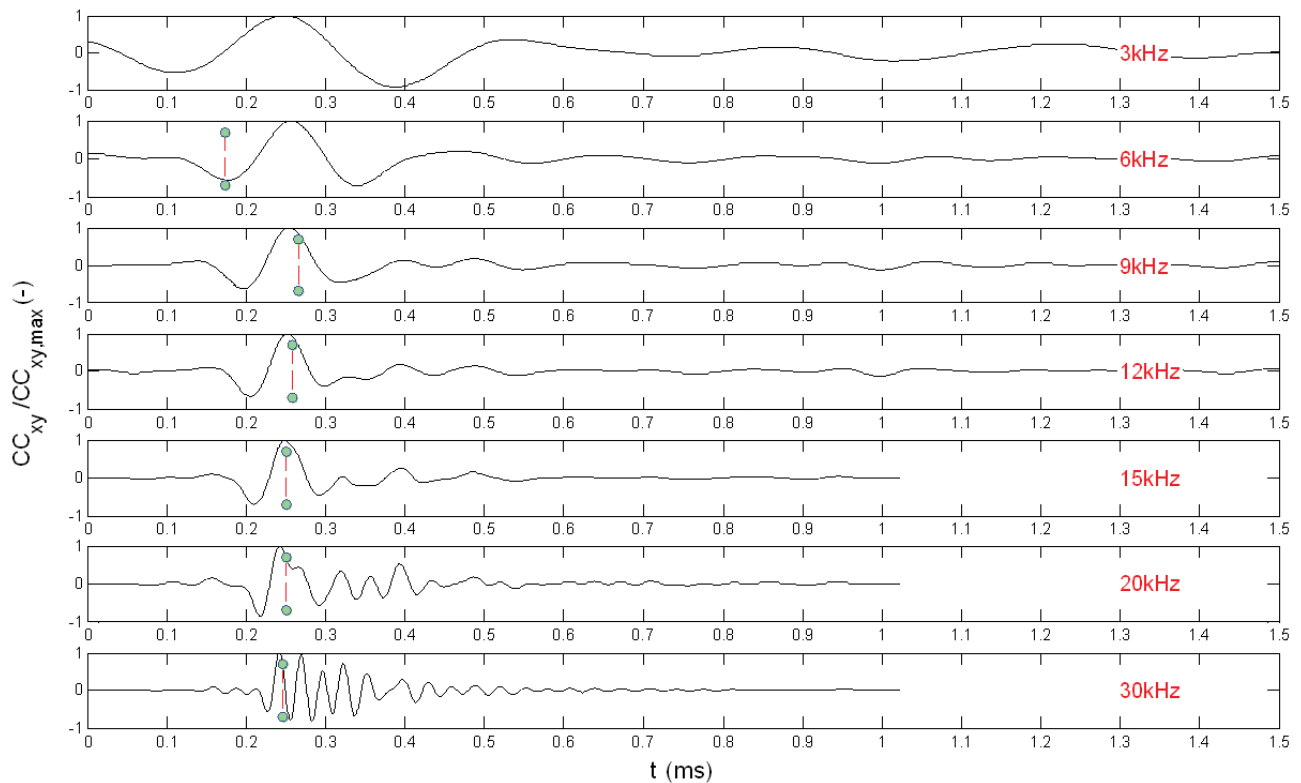


Figure 12. Normalised cross-correlation $CC_{XY} / CC_{XY,max}$ versus time for sample BO-I-J at $p' = 1300$ kPa.

The comparison of the interpretation using different techniques is presented and discussed in Section 5.

4 VARIATION OF G_0 VERSUS THE STATE OF BOŠTANJ SILTY SAND

In total, nine samples of Boštanj silty sand were prepared at different initial void ratios and isotropically compressed in triaxial apparatus. The bender-element tests were carried out with the aim to measure the variation of G_0 with the variation of density and the stress state of the sample during isotropic compression. The loading at higher stresses was employed in order to be able to reach the unique normal compression line (NCL) of the studied granular material (Coop [8]) and measure the G_0 values along it. The isotropic compression data of all the samples in the $e - \log p'$ plane are shown in Figure 13. It can be seen that by increasing the mean

effective stress p' , the isotropic compression lines start to converge towards a unique, straight, normal compression line (NCL) in the $e - \log p'$ plane. The proposed equation for the NCL is also shown on the plot. The bender element method was used to determine the values of G_0 along the isotropic compression lines and the results are shown in Figure 14. It can be seen from Figure 14 that decreasing the void ratio (e) causes the G_0 values to increase. Moreover, by increasing the stress p' the $\log G_0$ values in the $\log G_0 - \log p'$ plane tend to converge to a unique straight line, referred to as the $G_0(NCL)$ line. This line can be mathematically expressed in the form $G_0(NCL) = p_r A (p'/p_r)^n$, where the value of $A = 1459$ represents the intercept of the line and $n = 0.755$ its gradient, while p_r is a reference pressure of 1 kPa, used to make both parameters of the equation dimensionless. Similar observations were made on three other granular materials, as shown in Figure 15, i.e., Dogs Bay sand, Decomposed granite and Ham River sand by Jovičić and Coop [15].

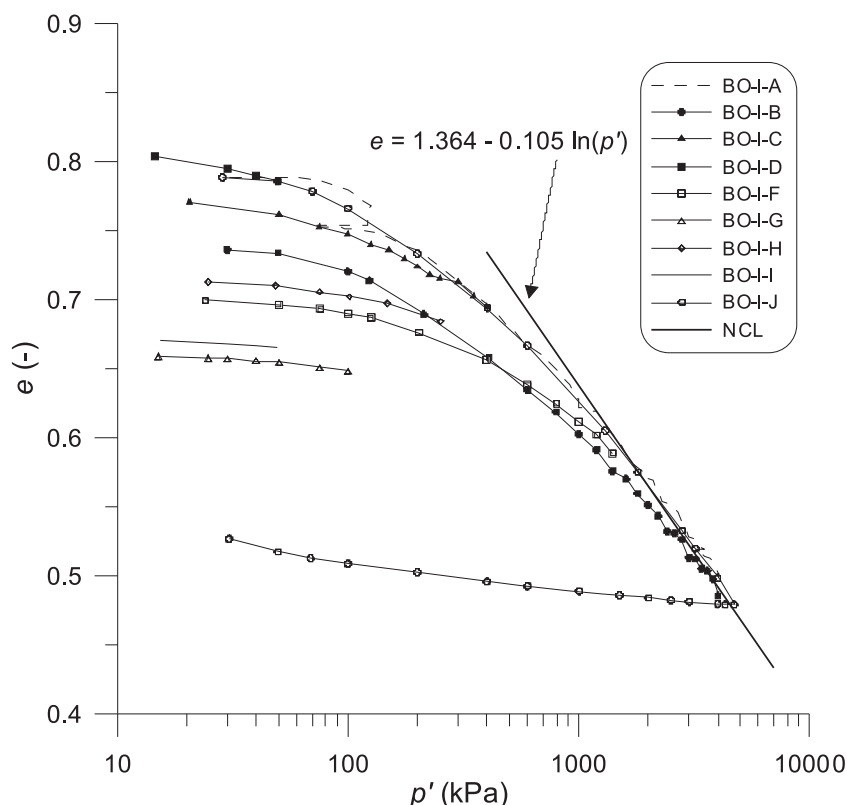


Figure 13. Isotropic compression of Boštanj silty sand in the $e - \log p'$ plane.

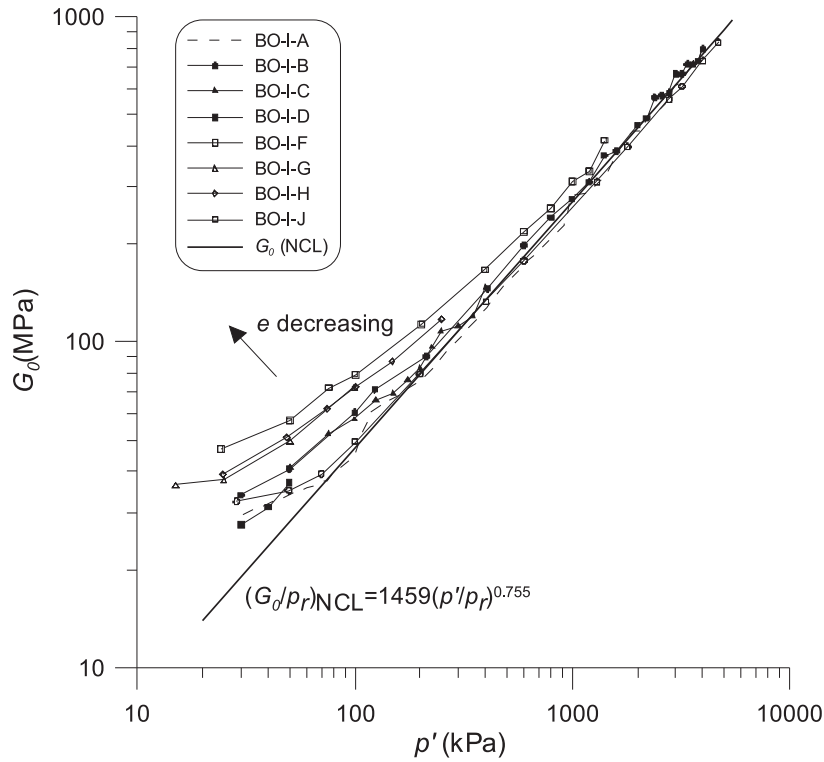


Figure 14. G_0 versus p' during isotropic compression first loading. The $G_0(NCL)$ line along with its equation is also shown on the plot. The G_0 values were calculated using the first-arrival method.

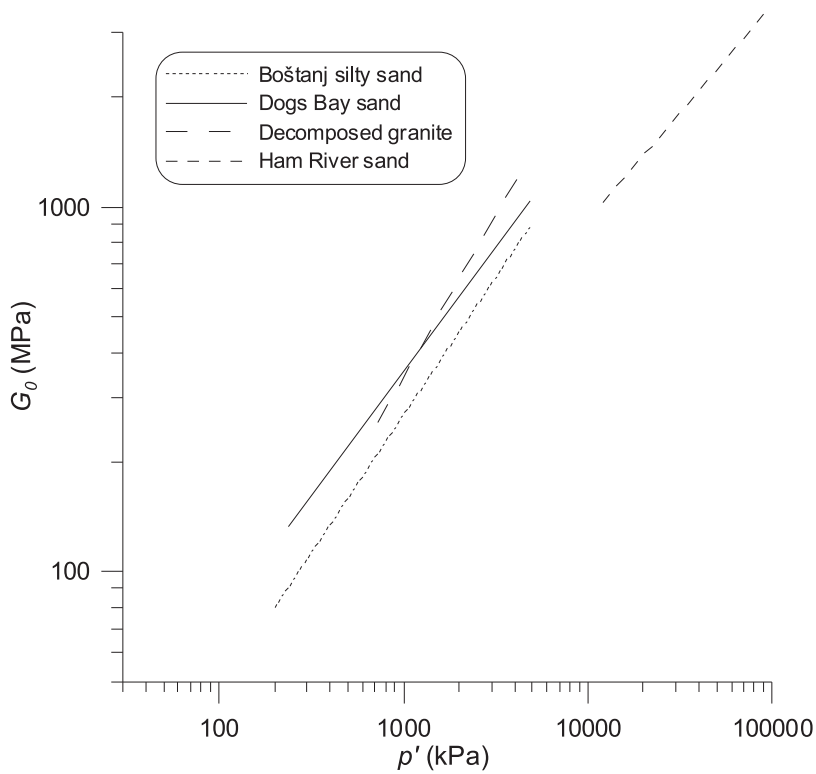


Figure 15. Comparison of G_0 values at NCL for different sands using the first-arrival method (data for Dogs bay sand, Decomposed granite and Ham River sand, after Jovičić and Coop [15]).

5 INTERPRETATION OF THE MEASUREMENTS USING DIFFERENT METHODS

The comparison of the G_0 values calculated using the first-arrival (TD), phase-change (FD) and cross-correlation (CC) methods for the two selected samples is shown in Figure 16. The sample BO-I-B was tested in the 5-MPa triaxial apparatus, while the sample BO-I-C was tested in the 0.8-MPa apparatus. It can be seen that the phase-change and cross-correlation methods give consistently lower values of G_0 compared to the first-arrival method. Moreover, the G_0 values of the phase-change and cross-correlation methods agree well with each other. Among all the tests, the differences between the first-arrival method and the other two methods are the biggest for the tests BO-I-C and BO-I-D, which suggests a system dependence of both methods, while all the other tests were performed in the 5-MPa apparatus.

If the phase-change results are plotted together, the convergence towards the linear trend at higher stresses is poorer compared to the first-arrival results (Figure 17 in

comparison with Figure 14), which is likely to indicate the higher level of inconsistency of the phase-change method compared to the first-arrival method. The same holds true for the cross-correlation method, which is known to be signal dependent.

To quantify the differences in the G_0 calculations using different methods, the relative error (E_r) in the G_0 calculation according to the three different methods is shown in Figure 18. The G_0 values derived using the first-arrival method are taken as reference values and E_r is calculated according to Equation (A.12). It can be seen that the relative errors in G_0 can be as high as 38%, which is significant. Furthermore, the relative errors for the phase-change, and also for cross-correlation method, are distinctively higher in the 0.8-MPa triaxial cell than in the 5-MPa cell. This difference in error shows the inconsistency of the phase-change and cross-correlation methods, according to the different system conditions (i.e., the different sample dimensions, the bender-element dimensions, the boundary conditions, etc.). Similar inconsistencies were also reported in the international inter-laboratory study of the ISSMGE [24], comparing different laboratories worldwide.

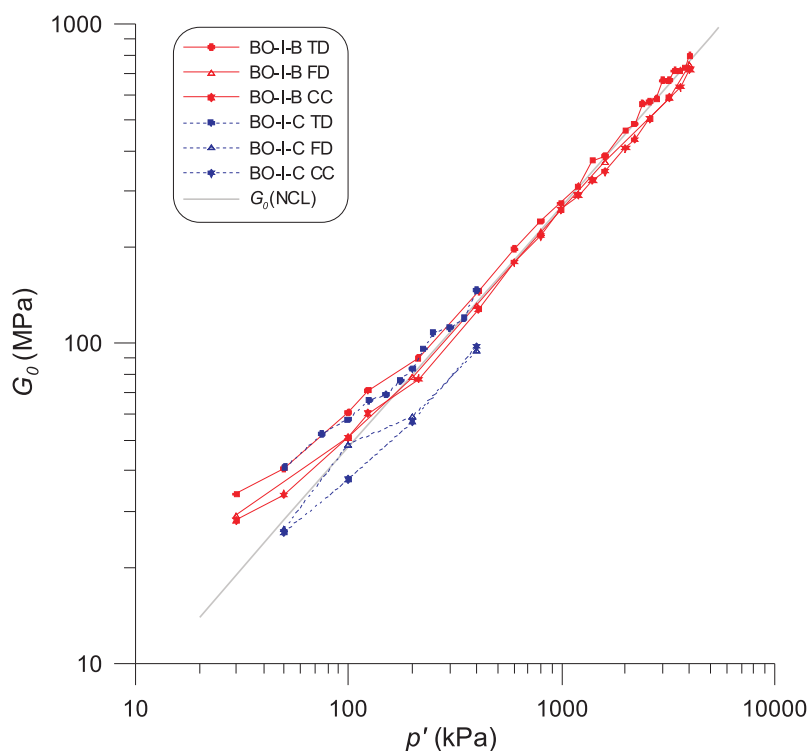


Figure 16. G_0 versus p' for samples BO-I-B and BO-I-C calculated using the first-arrival (TD), phase-change (FD) and cross-correlation (CC) methods.

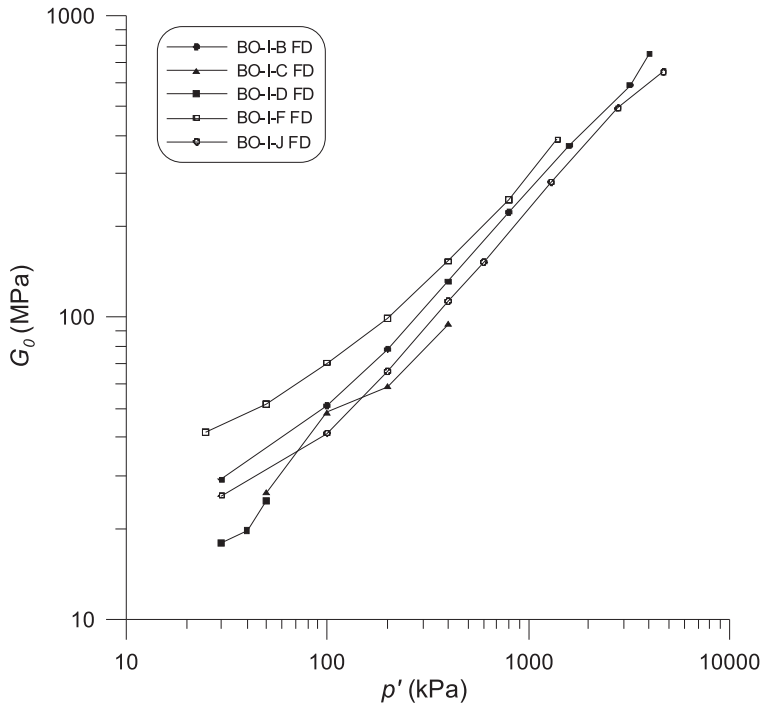


Figure 17. G_0 versus p' during isotropic compression first loading calculated using the phase-change method. The poorer convergence towards the linear trend with increasing p' can be seen according to Figure 14.

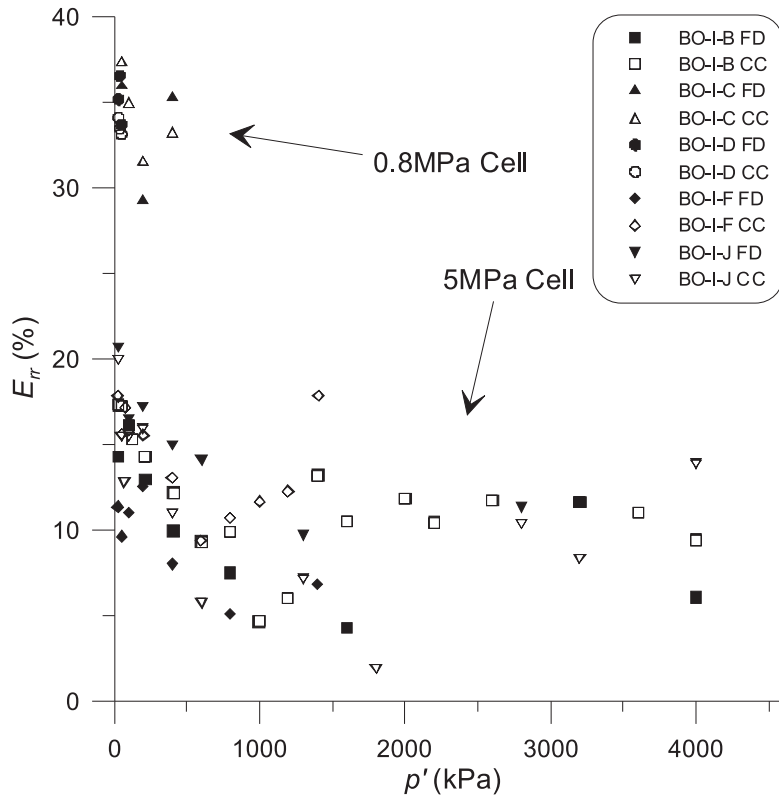


Figure 18. Relative errors E_{rr} in G_0 for the phase-change (FD) and the cross-correlation (CC) methods. The time-domain values are taken as reference values.

The values of G_0 measured by using the bender elements can be verified by employing other techniques for the shear-modulus determination, such as the resonant-column method, the shear-plates method, geophysical methods and static shear probes. All the samples of Boštanj silty sand were equipped with the local strain transducers. Therefore, a comparison between G_0 and the tangent shear stiffness of the static probes can be made. Figure 19 shows the tangent stiffness of the static shear probes from very small to large strains along with the G_0 measurements for all the samples. It can be seen that the G_0 values are higher than the tangent stiffness values at the initial stages of the tests at shear strain levels still reliably measured with static shear probes, which is in accordance with the expected material behaviour, while the G_0 is measured at lower strain levels than the tangent stiffness values at the initial stages of the tests.

6 DISCUSSION AND CONCLUSIONS

In accordance with the recommendations of the ISSMGE [24] and Fonseca et al. [12], three different methods for interpreting the G_0 values were employed in order to interpret the bender-element tests, i.e., the first arrival time, the cross-correlation and the frequency-domain method of phase change. The single-shot sine pulses were used as the driving signals for the time- and frequency-domain interpretations.

The deficiency of the frequency-domain (i.e., phase-change) method seems to be in the fact that the dispersion effects and multiple vibration modes mask the material response, which cannot be easily singled out from the phase-frequency relationship. Such techniques should probably also accommodate for the several frequency-response functions involved in the bender-

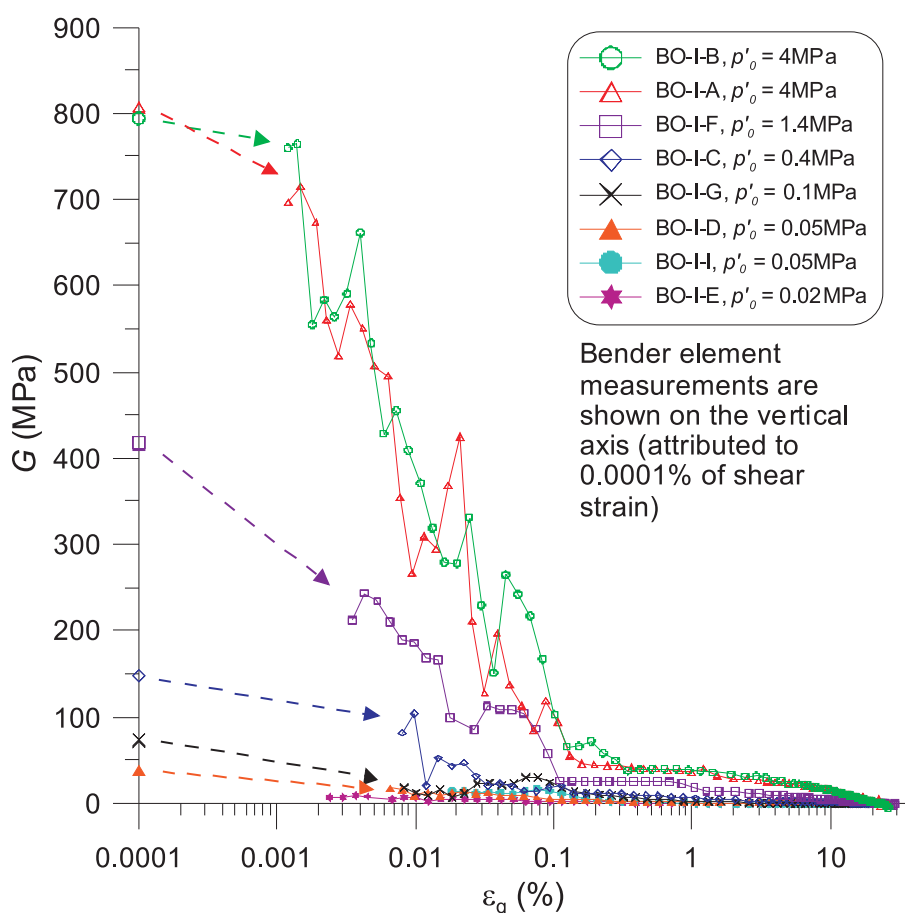


Figure 19. Dependence of the tangent shear stiffness G during the drained triaxial compression tests on the level of shear strain ε_q and the initial effective confining pressure p'_0 for Boštanj silty sand. For comparison, the values of the bender-element G_0 values are also shown in the figure for each sample.

element system to single out the frequency response function that is closer to the one of the soil (Lee & Santamarina [18]). Therefore, identifying the sharp time-arrival points in the time domain by visually inspecting many of the signals produced by pulse input sine signals at different excitation frequencies for samples of Boštanj silty sand was a more reliable approach than the one in the frequency domain.

The differences of G_0 calculated using the time and frequency domains can be very high (up to 38% of relative error), which is significant. The G_0 values calculated by the phase-change method are found to be consistently lower than the G_0 values from time domain. It seems to be a systematic difference, the reasons for which have not yet been fully understood [13,2,12]. One of the explanations is that both methods use the ready signal from the function generator as the transmitted signal, which is, in fact, not the signal that was transmitted to sample. The transmitted signal is the result of the interaction between the bender element and the soil at the time and the place of transmission and this cannot be determined without the use of a self-monitoring element (Jovičić [16]). Also, the phase-change and the cross-correlation methods are shown to be system dependent (type of signal, medium, boundary conditions, etc.) and are, as such, inconsistent.

Due to the reasons explained above, the results of the bender-element measurements were consistently interpreted using the time-domain method of the first arrival time. It was demonstrated that the samples of Boštanj silty sand converge during isotropic compression to a unique, linear, $G_0(NCL)$ line with an increasing mean effective stress p' . The comparable results and similar trends were also observed with the bender-element measurement for the three other granular materials, i.e., Dogs Bay sand, Decomposed granite and Ham River sand (Jovičić & Coop [15]). This demonstrates that in terms of the small strain stiffness, Boštanj silty sand, despite containing a relatively high percentage of non-plastic fines, follows the pattern of behaviour that is characteristic for sands in general.

APPENDIX

The shear-wave velocity is calculated according to the following relation

$$v_s = D/t_{arr}, \quad (A.1)$$

where D is the travelling distance of the wave and t_{arr} is its time arrival. The shear modulus G_0 at very small strains is calculated using the value of v_s and the bulk unit weight (ρ) as:

$$G_0 = \rho v_s^2. \quad (A.2)$$

The linear spectrum $L_x(f)$ of the signal $X(T)$ is its FFT into the complex field (e.g., Viggiani & Atkinson [23]) denoted by

$$L_x(f) = FFT[X(T)]. \quad (A.3)$$

The cross-power spectrum $G_{xy}(f)$ of the signals $X(T)$ and $Y(T)$ is

$$G_{xy}(f) = L_x(f) \cdot L_y(f)^*, \quad (A.4)$$

where $L_y(f)^*$ is a complex conjugate of the linear spectrum of $Y(T)$.

The transfer function $H(f)$ (frequency-response function) of the linear time invariable system is a vector in the complex domain. It can be written in complex polar notation [5] as:

$$H(f) = |H(f)| \exp(-j\phi(f)). \quad (A.5)$$

The absolute value $|H(f)|$ is termed as a system gain factor and the phase angle $\phi(f)$ as system phase factor. $|H(f)|$ denotes the ratio between the signal amplitudes

$$|H(f)| = \frac{|L_y(f)|}{|L_x(f)|}, \quad (A.6)$$

and the phase shift between the signals is equal to the phase factor as

$$\phi(f) = \phi_y(f) - \phi_x(f), \quad (A.7)$$

where ϕ_y and ϕ_x are the stacked phases of the signals $X(T)$ and $Y(T)$.

The phase velocity ($v_{ph}(f)$) of each frequency component can be calculated from the secant of the plot $f - \phi$ as

$$v_{ph}(f) = 2\pi D \frac{f}{\phi(f)}, \quad (A.8)$$

where D is the travelling distance of the travelling wave. The group velocity (v_g) of the wave packet from the chosen frequency interval is calculated from the slope of the tangent $\frac{df}{d\phi}$ from this frequency interval as

$$v_g = 2\pi D \frac{df}{d\phi}. \quad (A.9)$$

If the system was non-dispersive, which is not the case in real bender-element systems, the values of the phase and group velocities would be equal. Of greater practical application is the group time arrival (t_g) of the wave packet from the chosen frequency interval, defined as

$$t_g = \frac{1}{2\pi} \frac{d\phi}{df}. \quad (\text{A.10})$$

In the following, the definition of the cross-correlation function $CC_{xy}(t)$ is given. It is a measure of the degree of correlation of the two signals $X(T)$ and $Y(T)$ and is analytically defined [23] as

$$CC_{XY}(t) = \lim_{T_r \rightarrow \infty} \frac{1}{T_r} \int_{T_r} X(T)Y(T+t)dt, \quad (\text{A.11})$$

where T_r is the length of the sampled signals and t is the time shift between the signals.

The relative error E_{rr} of the G_0 calculation using the phase-change or cross-correlation methods ($G_{0,i}$) according to the G_0 value of the first-arrival method ($G_{0,FA}$) is calculated as

$$E_{rr} = \frac{G_{0,FA} - G_{0,i}}{G_{0,FA}}. \quad (\text{A.12})$$

ACKNOWLEDGMENTS

The research presented in this paper was performed at Imperial College Soil Mechanics Laboratory, London. The authors are grateful to Professor Matthew Coop at Imperial College and Doctor Giovanni Alvarado from Geotechnical Consulting Group, London (formerly a PhD student at Imperial College) for their help and support in measuring, numerical and interpretational issues. The financial support of Imperial College, the Ministry of Higher Education, Science and Technology of the Republic of Slovenia, the AdFutura scholarship fund and the Slovenian National Building and Civil Engineering Institute (ZAG Ljubljana) is gratefully acknowledged.

REFERENCES

- [1] Alvarado, G. (2007). *Influence of late cementation on the behaviour of reservoir sands*. PhD Thesis, Imperial College, University of London.
- [2] Alvarado, G., Coop, M.R. (2004). Experience of bender element measurements on a variety of materials. *Workshop on Bender Element Testing of Soils*, University College, London.
- [3] Arroyo, M., Muir Wood, D., Greening, P.D., Medina, L., Rio, J. (2006). Effects of sample size on bender-based axial G_0 measurements. *Géotechnique*, 56(1), 39-52.
- [4] Arroyo, M., Muir Wood, D., Greening, P.D. (2003). Source near-field effects and pulse tests in soil samples. *Géotechnique*, 53(3), 337-345.
- [5] Bendat, J.S., Piersol, A.G. (2000). *Random data: analysis and measurement procedures*. John Wiley & Sons.
- [6] Brignoli, E.G.M., Gotti, M., Stokoe, K.H. (1996). Measurement of shear waves in laboratory specimens by means of piezoelectric transducers. *Geotechnical Testing Journal*, 19(4), 384-397.
- [7] Brignoli, E.G.M., Gotti, M. (1992). Misura della velocità di onde elastici di taglio in laboratorio con l'impiego di traduttori piezoelettrici. *Riv. Ital. Geotec.* 26, 1, 5-16.
- [8] Coop, M.R. (2003). On the mechanics of reconstituted and natural sands. Keynote lecture. In: Di Benedetto, H., Doanh, T., Geoffroy, H., Saueat, C. (eds.). *Deformation Characteristics of Geomaterials*. Swets and Zeitlinger, Lisse, Vol. 2, 29-58.
- [9] Cuccovillo, T., Coop, M.R. (1997). The measurement of local axial strains in triaxial tests using LVDTs. *Géotechnique*, 47, 1, 167-171.
- [10] Dyvik, R., Madshus, C. (1985). Lab measurements of G_{max} using bender elements. In: *Proc. of the ASCE Conference on Advances in the Art of Testing Soils under Cyclic Conditions*, Detroit, 186-196.
- [11] Fernandez, A.L. (2000). *Tomographic imaging the state of stress*. PhD Thesis, Civil Engineering, Georgia Institute of Technology, Atlanta.
- [12] Fonseca, A.V., Ferreira, C., Fahey, M. (2009). A framework interpreting bender element tests, combining time-domain and frequency-domain methods. *Geotech. Testing J.*, 32, 2, 91-107.
- [13] Greening, P.D., Nash, D.F.T. (2004). Frequency domain determination of G_0 using bender elements. *Geotechnical Testing Journal*, 27, 3, 288-294.
- [14] Jardine, R.J., Shibuya, S. (2005). TC29 workshop: Laboratory tests. Report. *Proc. of the 16th International Conference on Soil Mechanics and Geotechnical Engineering*, Osaka 5, 3275-3276.
- [15] Jovičić, V., Coop, M.R. (1997). Stiffness of coarse-grained soils at small strains. *Géotechnique*, 47(3), 545-561.
- [16] Jovičić, V. (1997). *The measurement and interpretation of small strain stiffness of soils*. PhD thesis, The City University, London.

- [17] Jovičić, V., Coop, M.R., Simić, M. (1996). Objective criteria for determining G_{max} from bender element tests. *Géotechnique*, 46(2), 357-362.
- [18] Lee, J-S., Santamarina, J.C. (2005). Bender elements: performance and signal interpretation. *Journal of Geotechnical and Geoenvironmental Engineering*, 131, 9, 1063-1070.
- [19] Lenart, S. (2008). The response of saturated soils to a dynamic load. *Acta Geotechnica Slovenica*, 5, 1, 37-49.
- [20] Rio, J.F.M.E. (2006). *Advances in laboratory geophysics using bender elements*. PhD thesis, University College, London.
- [21] Sánchez Salinero, I., Roesset, J.M., Stokoe, K.H. (1986). Analytical studies of body wave propagation and attenuation. Geotechnical Engineering Report No. GR86-15, Civil Engineering Department, University of Texas at Austin.
- [22] Shirley, D.J., Hampton, L.D. (1977). Shear wave measurements in laboratory sediments. *J Acoust Soc Am*, 63(2), 607-613.
- [23] Viggiani, G., Atkinson, J.H. (1995). Interpretation of bender element tests. *Géotechnique*, 45(1), 149-154.
- [24] Yamashita, S., Fujiwara, T., Kawaguchi, T., Mikami, T., Nakata, Y., Shibuya, S. (2007). International parallel test on the measurement of G_{max} using bender elements. Organized by Technical Committee 29 of the ISSMGE (<http://www.jiban.or.jp/e/tc29>).